

Two-dimensional inductively coupled argon plasma simulations with experimental verification

WEN-FENG. ZHAO*, ZHOU. YANG, JUN-FANG. CHEN^a

College of Engineering, south china agricultural university, Guangzhou, 510642, People's Republic of China

^aSchool of Physics and Telecommunication Engineering, Laboratory of Quantum Information Technology, South China Normal University, Guangzhou, China, 510006, People's Republic of China

A two-dimensional model has been developed for simulating the behavior of inductively coupled plasma torches by using customized computational fluid dynamic (CFD) commercial CFDRC software. Both Ar⁺ (the argon ion) and Ar^{*} (the metastable argon atomic) distributions in inductively coupled plasma are presented from this simple model. The optical emission spectroscopy and Langmuir probe are applied to analyze the characteristic of Ar plasma and verify the model. The results show that the predictions seem to be reasonable fundamentally and are similar with Optical Emission Spectroscopy and Langmuir probe observation in some aspects including the Ar^{*} distributions and flow vortexes influence. Due to the model contains several simplification, some differences appear by mean of comparing calculated with measured Ar⁺ distributions.

(Received July 20, 2012; accepted September 20, 2012)

Keywords: Inductively coupled plasma; Emission spectroscopy; Single Langmuir probe; Simulation

1. Introduction

Inductively coupled plasma (ICP) is often of particular interest because they can provide charged particles with high density and low electron temperature, which can minimize the contamination to the substrate [1]. This makes ICP sources most attractive [2]. Then plasma reactors are widespread in industry for both material processing and synthesis [3]. It is essential to measure and optimize parameters of plasma in order to improve the processing characteristics of the discharge through understanding of the physics involved [4][5]. Process uniformity is a key requirement to enable large wafers or flat panels to be processed by plasma [6].

Optical Emission Spectroscopy (OES) is the most popular technique to investigate glow discharge since it is simple and produces no perturbation in the plasma [7]. Langmuir probe is a simple but valuable technique employed to characterize the plasma parameters. The I-V characteristic obtained from the data can be used to determine the electron temperature and the ion density [8]. Many research groups have the radial and axial distribution of ion densities in many sorts of inductively coupled plasma reactors with different gases and conditions [9].

Mathematical modeling is a powerful tool to deeply investigate physical and chemical phenomena occurring within inductively coupled plasma torches. Various numerical models with increasing complexity have been proposed over the years with the aim of obtaining a more and more realistic prediction of plasma behavior and chemical processes inside the torch [10]. Computational Fluid Dynamic (CFD) approach offers important advantages in modeling, such as the possibility of studying

complicated geometries, using different physical and numerical models and easily generating both structured and unstructured meshes [11]. Computational fluid dynamics is also a discipline that encompasses the numerical solution of the equations of motion (mass, momentum and energy) in a flow geometry of interest, together with subsidiary sets of equations reflecting the problem at hand [12]. Several publications describe plasma modeling and spatial distributions of ion density [13]. Kushner (2009) discussed the basis and implementation of Hybrid modelling using examples from studies of ICP reactors. Hybrid modelling has demonstrated the ability of addressing a variety of reactor types and physical processes [14].

The commercial software package, CFD-ACE+ (ESI-CFD Inc., Huntsville, USA) has been used to perform the simulations. The radial distribution property of argon plasma is investigated by single Langmuir probe in ICP instrument. A comparison between Langmuir probe measurements, OES and numerical simulations is made in this work in ICP instrument.

2. Theory

2.1 Plasma model

2.1.1 Assumptions

The Plasma module implemented in CFD-ACE+ is based on the solution of the fluid equations (moment equations derived from Boltzmann equation with the assumption of Maxwellian energy distribution) for electron and heavy (ions and neutrals) particle transport, in

conjunction with the electro-magnetic field solved in electric and magnetic modules of CFD-ACE+. Ion transport in plasma is solved from the drift-diffusion equations.

The CFD numerical simulation is based on the following assumptions: (1) the electron density is derived from the quasi-neutrality condition; (2) the fluid flow is axisymmetric and steady-state; (3) the sheath is negligibly thin and no net conduction current is present in plasma.

2.2.2 Governing equations

Electromagnetic field treatment is as follows:

The electric field is defined as

$$\vec{E} = -\frac{\partial \vec{A}}{\partial t} - \nabla \phi \quad (1)$$

Where ϕ is electric potential, $-\nabla \phi$ is the electrostatic field, \vec{A} is the magnetic vector potential. They can be got by using the finite volume method (FVM) to solve Maxwell equations in the frequency domain.

The equation is found as follows:

$$\frac{1}{\mu_0 \mu_r} \nabla^2 \vec{A} = -\varepsilon_r \varepsilon_0 \frac{\partial^2 \vec{A}}{\partial t^2} + \varepsilon_r \varepsilon_0 \frac{\partial \nabla \phi}{\partial t} + \sigma \cdot \frac{\partial \vec{A}}{\partial t} + \sigma \nabla \phi - \sigma \cdot \vec{u} \times \vec{B} - \vec{J}_s \quad (2)$$

In the frequency domain equation (2) becomes

$$\frac{1}{\mu_0 \mu_r} \nabla^2 \vec{A} = -\varepsilon_r \varepsilon_0 \omega^2 \vec{A} + j\omega \varepsilon_r \varepsilon_0 \nabla \phi + j\omega \sigma \vec{A} + \sigma \nabla \phi - \sigma \cdot \vec{u} \times \vec{B} - \vec{J}_s \quad (3)$$

Where μ_0 is the permeability of the free space, μ_r is the relative permeability, ε_0 is the electric permittivity of the free space, ε_r is the electric relative permittivity, \vec{u} is the fluid velocity vector, σ is the electric conductivity, \vec{B} is magnetic field intensities, $\sigma \cdot \vec{u} \times \vec{B}$ is the convective and \vec{J}_s is the current of user self-defining. The Current of each electro magnetic source will be automatically and proportionally adjusted to achieve the specified power absorption in the plasma in magnetic module.

The electron temperature T_e from the electron energy balance is as follows:

$$\frac{3}{2} \frac{\partial}{\partial t} (n_e T_e) + \nabla \cdot \left(\frac{5}{2} T_e \vec{\Gamma}_e - \frac{5}{2} n_e D_e \nabla T_e \right) = P_{joule} + P_{ind} = P \quad (4)$$

The drift diffusion approximation is used for the electron density flux:

$$\vec{\Gamma}_e = \mu_e n_e \vec{E} - D_e \nabla n_e \quad (5)$$

The power density, P , stands for the energy absorbed by electrons, such as Joule heating ($P_{joule} = e \vec{\Gamma}_e \cdot \vec{E}$), inductive heating ($P_{ind} = \frac{1}{2} \text{Re} \left\{ \vec{j}_e \cdot \vec{E} \right\}$).

Where $\vec{\Gamma}_e$ is electron density flux, n_e is electron density, \vec{E} is the electric potential, D_e is electron diffuse coefficient and L is the electron energy loss due to the electron induced reactions.

In the presence of charged species (ions, metastables), the mass flux of each species is as follows:

$$\vec{J}_i = -\rho D_i \nabla Y_i + \rho Y_i \vec{u}_{di} + \vec{J}_c \quad (6)$$

$$\vec{u}_{di} = \vec{E} (q_i \mu_i - \sum_j q_j \mu_j Y_j) \quad (7)$$

Where mass fraction Y_i is the mass fraction, ρ is mass density, D_i is the diffusion coefficient, \vec{u}_{di} is the drift velocity, μ_i is the mobility of charged particles. The flux \vec{J}_c appears as a result of the Stefan-Maxwell procedure to satisfy the mass conservation, $\sum_i \vec{J}_i = 0$.

2.2.3 Boundary conditions

The velocity of neutral species at the boundary corresponds to thermal velocity, $(RT/2\pi m_i)^{1/2}$. The velocity of ions is determined by the local value of the electric field. In most cases, zero electron density at the walls is appropriate.

Under Plasma options ICP, the substrate holder, outlet and inlet are setup as thermal flux balance. The implementation of the wall is fix gradient at zero. The fixed gradient at zero value means that no electron energy is lost at the boundary. The thermal flux balance allows the energy loss limited by thermal flux.

2.2.4 Gas reaction

The chemical reactions included in the model are shown in Table 1 [15]. The model contains four species: electrons, positive argon ions, ground state argon neutrals, and a single argon metastable species.

Table 1. Gas-phase reaction for argon plasma

Chemical reaction	Reaction rate
Ionization & excitation	
$Ar + e \rightarrow Ar^+ + 2e$	Cross section from JILA
$Ar + e \rightarrow Ar^* + e$	Arrhenius type
$Ar^* + e \rightarrow Ar^+ + 2e$	Arrhenius type
Elastic collision	
$Ar + e \rightarrow Ar + e$	Cross section from JILA

2.2.5 Surface reaction

The rate of surface reaction is defined by sticking coefficient [15]. The surface reaction of argon main is combination reaction in the surface of substrate or wall. The reaction is as follows:



The Ar^+ is the argon ion and the Ar^* is the metastable argon atomic.

3. Experimental

We consider a cylinder with a planar three-turn loop antenna. The cylinder chamber has dimensions of 25 cm in height and 10 cm in radius. The quartz window with the thickness of 2 cm is inside the chamber. The antenna is located at $r = 10$ cm along the axis. The schematic diagram of the experimental setup is illustrated in Fig.1. The plasma is generated in the quartz discharge chamber with the help of a 13.56 MHz RF generator and an automatic impedance matching network with a spiral configuration of copper electrodes of diameter 6 mm. The plasma diffuses and enters a cylindrical stainless steel vacuum chamber. The flow of Ar gas is monitored with mass flow meters whereas pressure in the chamber is recorded by using gauge.

The optical emission spectrometer is composed of optical collection system, monochromator and photo-electronic acquisition system. After being amplified by a direct-current (DC) amplifier, the output signal of the photoelectron multiplication tub (PMT) is transmitted to a computer for acquisition. The wavelength range of the monochromator is 200–660 nm and its highest resolution is 0.1 nm.

A single Langmuir probe is inserted in the chamber in order to measure the ion density. The inflectional probe with a diameter of 0.5 mm is shown in Fig.1. The radial position at $r=0, 2, 4, 6$ cm can be acquired by revolving the probe head according to the calculated angle. The axial position at $h=0.5, 3, 7, 10$ cm can be reached by adjusting the height of probe. The I-V characteristic curves are obtained by using a power supply. All calculations of

plasma parameters are performed through a PC by using suitable software. By recording the current through Langmuir probe as a function of the applied voltage, the I-V characteristic is obtained and the data is used to calculate ion density. The electron temperature KT_e , is determined in electron volts by the equation

$$KT_e = [\Delta(I_e/\Delta V)]^{-1} \quad (10)$$

The ion density (n_i) is obtained from the electron saturation current using the equation

$$I_e = Aen_i(KT_e/2\pi m)^{1/2} \quad (11)$$

Where A is the probe area, e is the magnitude of the electronic charge, m is the electronic mass and K is the Boltzmann constant [16].

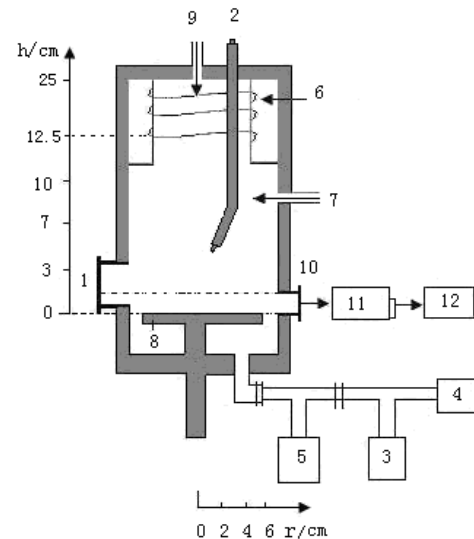


Fig. 1. The schematic construction of the experiment 1—Observation window ;2—Langmuir probe ;3—Valve ; 4—vacuum pumps ; 5—vacuum gauge ; 6—RF electrode coil; 7—gas supply 1; 8—Substrate holder 9—gas supply 2; 10—the window for OES measurement ; 11—Monochromator ; 12—computer.

4. Results and discussion

4.1 Radial distribution profile by model

The calculated ion density (charge pressure: 0.5 Pa, plasma power: 120 W) in Fig.2 exhibits the typical profile [17]. The maximum value of the argon ion, Ar^+ , and the metastable argon atomic, Ar^* , appears just in the center of the reactor. It is interesting to note that the value ranges from $2 \times 10^9 \text{ cm}^{-3}$ to $1.75 \times 10^{10} \text{ cm}^{-3}$ and from $1 \times 10^{11} \text{ cm}^{-3}$ to $7.667 \times 10^{11} \text{ cm}^{-3}$, respectively. The walls of the discharge chamber as sinks of charged particles; electrons are absorbed at the walls, and ions are converted into neutrals. As a result, plasma density is spatially non-uniform

exhibiting a maximum in the center. According to reference [18], the decrease of the electron density from the center towards the boundaries may be caused by the confinement of electrons with a low total energy.

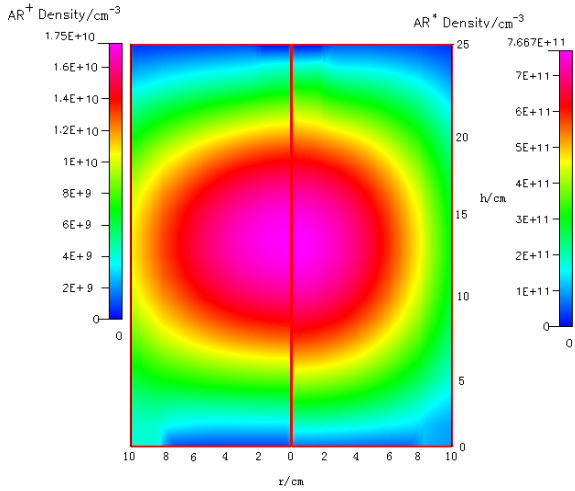


Fig. 2 Ar^+ and Ar^* density distributions calculated by modeling

It is well known that Ar^* is generated at the first excitation energy (11.55 eV) and Ar^+ is produced at the ionization energy (15.76 eV) [19]. We can see that the excitation potential of Ar^* is lower than that of Ar^+ . The bulk of the particles have a low energy while a small fraction has a much higher energy [20]. So the Ar^* density is several ten times of Ar^+ density.

4.2 OES experiment verification

For verification of the calculated result, we first examined the ratio of Ar^* to Ar^+ by OES then diagnosed the ion density radial distribution by Langmuir single probe.

The effects of radiofrequency (RF) power on the intensity of the spectra at the location $h=0.5\text{cm}$ were investigated, as shown in Fig.3 with keeping the total pressure at 0.5 Pa.

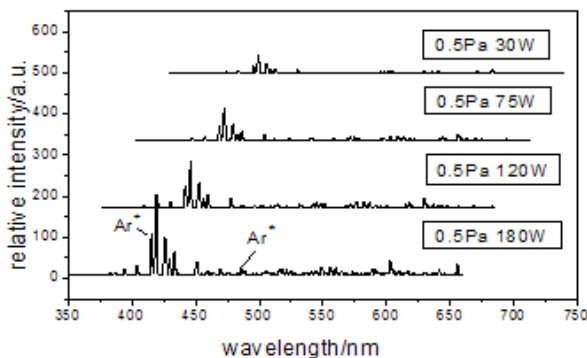


Fig.3 Optical emission spectra of Ar plasma

The emission intensity of particular wavelength from an excited state is proportional to the concentration of species in that excited state [21]. The optical emission spectra shows that the intensity of emission increases linearly with RF power. Increase of RF power causes more ionization, which in turn increases the population of various energy levels associated with the ions leading to the increase in integral intensity.

It can be seen in this spectra the relative intensity of low excitation state of argon atomic (415.5 nm) is higher than that of high excitation state of argon ion (488 nm). The reason is that the electron energy is not high enough to excite the high level spectrum line in ICP [22].

Due to the lack of the method of directly measuring Ar^* density, we adopted ratio of argon atomic (415.5 nm) line intensity to argon ion (488 nm) line intensity measured by OES, $I_{415.5}/I_{488}$, as the index of the ratio of Ar^* density to Ar^+ density, Ar^*/Ar^+ . Namely, the value of $I_{415.5}/I_{488}$ should be proportional to the value of Ar^*/Ar^+ . The comparison result is investigated under different RF power and shown in Fig. 4, in which the discharge pressure is 0.5 Pa.

The calculated value, Ar^*/Ar^+ , and the experiment value, $I_{415.5}/I_{488}$, are basically proportional and the ratio keeps constant under different powers. It proves to some extent, that the calculated Ar^* density is reliable. Though the electron energy distribution function (EEDF) is non-Maxwellian for the lower pressure discharge, electron, fast argon ion, and especially fast argon atom impact excitation from the ground state are important production processes [23]. Then in the numerical model, the assumption of Maxwellian electron energy distribution has a slightly effect on the distribution of Ar^+ density.

From Fig. 4 we can also see the two lines are not parallel complete. The electron density increases with increasing of the RF power. Then EEDF tends to Maxwellian distribution from non-Maxwellian while the increasing of the electron density [24]. Since the EEDF transforms, the $I_{415.5}/I_{488}$ also changes. So the result of numerical model which assumes Maxwellian distribution is slightly different with the OES.

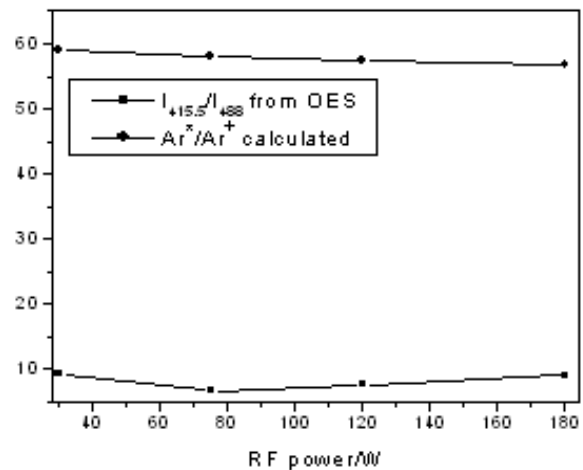


Fig. 4 The comparison spectral line $I_{415.5}/I_{488}$ measured from OES with Ar^*/Ar^+ calculated

4.3 Langmuir probe verification

We compared the calculated ion densities to those experimentally measured. Fig.5 (a) and (b) show the two-dimensional distributions of the ion density (based on four lateral profiles at $h=0.5, 3, 7, 10$ cm). It is observed that the charged particle density is rather uniform in the radial direction from $z=0$ to $z=6$ cm.

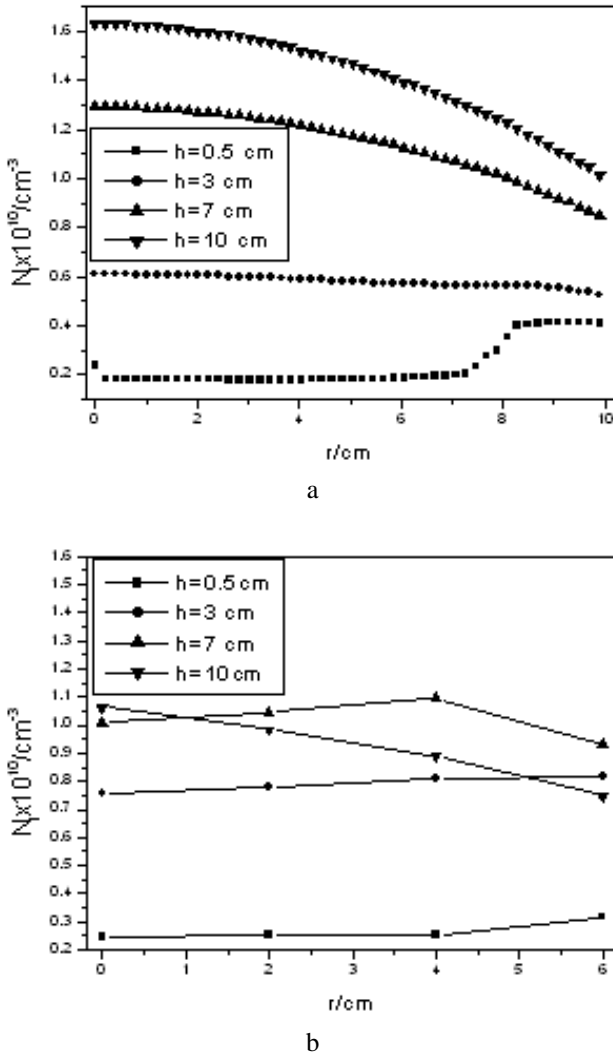


Fig.5 (a) The Ar^+ density radial distribution calculated under discharge pressure 0.5 Pa and RF power 120 W. (b) The Ar^+ density radial distribution measured under discharge pressure 0.5 Pa and RF power 120 W.

In comparing the calculated values to the experimentally measured ones, it becomes clear there is good agreement between the model's predictions and the experimental measurement at $h=0.5$ cm and $h=3$ cm. Due to the limitation of probe shape, we can not measure the ion density from $r=6$ cm to $r=10$ cm. Then the model gives the detail distribution in the region. We can also see the calculated value approach each other from $r=6$ to $r=10$ cm. It can be observed at $r=6$ cm in experimental value, too. These changes are generated by flow vortices at the plasma outlet, which has been already reported by several

authors [25]. There is a short distance between substrate holder and outlet in our equipment but it does not appear in the model. The flow vortices can be generated. The flow vortices absorb more energy from antenna and disturb uniform distribution of ion density. These make the ion density increase at the position.

Additional, calculated data are larger at $h=7$ cm and $h=10$. There are several points to make. Firstly, the actual absorbed power is less than the input power of the power supply since the supplied RF power is partly reflected and dissipated in the antenna. Secondly, there is energy losses associated with the various species, which are not considered by the numerical model [26].

However, we note that the peak values of calculated data appear at $h=10$ cm while those of experimental data at $h=7$ cm. Some shortcoming can be neglected on plasma parameters, for example the wall of reactor is composed of quartz (location from $h=9$ cm to $h=25$ cm) and stainless steel (location from $h=0$ cm to $h=9$ cm) in our equipment but the wall is only quartz in numerical model. Metal can reflect electromagnetic waves, resulting in the energy can be reabsorbed by plasma. So the maximum value appears at lower ($h=7$ cm) location.

If the plasma model is applied to real processes, all assumptions which are made on plasma symmetry, coil geometry, plasma radiation are only approximate. The experiment equipment is not symmetrical completely which includes observation window and the window for OES measurement. That leads that Langmuir probe measurements have an off-axis maximum for the ion density at some location ($h=7$ cm).

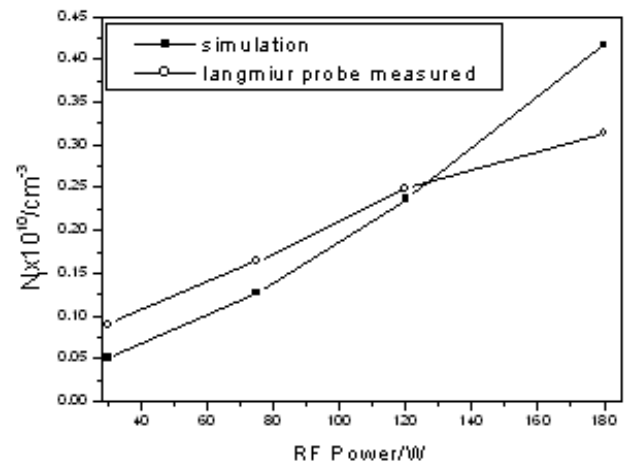


Fig.6 Variation of ion density calculated and measured of various power at discharge pressure of 0.5 Pa.

Fig.6 shows the ion density profiles of simulation and experiment at various powers at the location $h=0.5$ cm and $r=0$ cm. The ion density is found to increase greatly with increase of RF power. The signal is agree with the result of OES above. The ion density n_i is as follow

$$n_i = P_{\text{abs}} / (eU_B A_{\text{eff}} \varepsilon_T) \quad (12)$$

where P_{abs} is the excited power, U_B is the Bohm speed, e is the magnitude of the electronic charge, A_{eff} is the loss effect area of particle, and ε_T is the energy of Particle. From this equation, we can see the ion density also increases linearly with power [24].

5. Conclusions

A two-dimensional model has been developed for simulating the behavior of inductively coupled plasma torches, using customized CFD commercial code CFDRC (CFDRC research corporation, Huntsville, USA). Calculation of Ar^+ and Ar^* density distributions of an inductively coupled plasma are presented. The predictions seem to be reasonable fundamentally and are similar with OES and Langmuir probe observation in some aspects. The Ar^* density is several ten times of Ar^+ density. The ICP plasma has fine uniformity and the ion density reaches about $1.75 \times 10^{10} \text{ cm}^{-3}$ under RF power 120 W and discharge pressure 0.5 Pa. The flow vortexes can affect the Ar^+ distribution at the plasma outlet.

Due to the model contains several simplifications, the measured Ar^+ distributions reveal that an off-axis maximum in some location is generated and the peak value appears at lower location. These are not observed by calculated distribution. The model and verification methods seems to not to sufficient to describe the density distributions exactly then it is necessary to improve the model and study the OES further.

The inductively coupled Ar plasma by means of optical emission spectroscopy (OES) is studied under different conditions which show the relative intensity of low excitation state of argon atomic (415.5 nm) is higher than that of high excitation state of argon ion (488 nm).

Changing the RF power, the probe analysis shows that the ion density increases linearly with the increasing of the RF power.

Acknowledgments

This work was supported by Foundation for Distinguished Young Talents in Higher Education of Guangdong, China (LYM11031) and Guangdong Province Science and Technology Department Project (2011B050100013).

References

- [1] K. H. Bai, D. S. Lee, H. Y. Chang, *Appl. Phys. Lett.* **80**, 3907(2002).

- [2] W. Zhao, J. Chen, S. Song et al., *Optoelectron. Adv. Mater. – Rapid Comm.* **5**(3),231 (2011).
- [3] M. Brinza, J. K. Rath, R. E. I. Schropp, *Solar Energy Materials & Solar Cell*, **93**, 680 (2009).
- [4] Lee Min-Hyong, Jang Sung-Ho, Chung Chin-Wook, *Phys. Plasmas*, **13**, 053502 (2006).
- [5] V. Carcelén, N. Vijayan, E. Diéguez, A. Zappettini, et al., *J. Optoelectron. Adv. Mater.* **10**(11),3135(2008).
- [6] Park Se-Geun, Kim Chul, O Beom-hoan, *Thin Solid Films*, **355-356**, 252(1999).
- [7] F. Liu, C. S. Ren, Y. N. Wang, et al., *Vacuum*, **81**, 221(2006).
- [8] A. Okada, K. Kijima, *Vacuum*, **65**, 319(2002).
- [9] U. S. Okuji, N. Sakudo, K. Hayashi, et al., *Surface and Coatings Technology*. **136**,102 (2001).
- [10] H. C. Kim, F. Iza, S. S. Yang, M. Radmilović-Radjenović, J. K. Lee, *J. Phys. D: Appl. Phys.* **38**, 283 (2005).
- [11] A. P. Sichler, S. Büttgenbach, L. Baars-Hibbe, *Chemical Engineering Journal*, **101**, 465 (2004).
- [12] D. Jegger, S. Sundaram, K. Shah, *Perfusion*, **22**, 257(2007).
- [13] Tae Won Kim, Eray S. Aydil, *J. Appl. Phys.* **92**(11), 6444(2002).
- [14] Mark J Kushner., *J. Phys. D: Appl. Phys.* **42**, 194013(2009).
- [15] Cheng Jia, Zhu Yu, Wang Jinsong. *Chinese Journal of Semiconductors*, **28**(6), 989 (2007).
- [16] Qayyum Abdul, Ikram M, Zakaullah M, *International Journal of Modern Physics B*, **17**(14), 2749(2003).
- [17] U. Kortshagen, I. Pukropski, M. Zethoff, *J. Appl. Phys.* **76**(4), 2048 (1994).
- [18] Mu`mken G, Kortshagen U, *J. Appl. Phys.* **80**(12), 6639(1996).
- [19] ChinWook Chung and Hong-Young Chang, *Phys. Plasmas*, **7**, 3826 (2000).
- [20] T. Hori, M. D. Bowden, K. Uchino, K. Muraoka, *Appl. Phys. Lett.* **69**(24), 3683 (1996).
- [21] Davide Mariotti, Yoshiki Shimizu, Takeshi Sasaki, et al., *Appl. Phys. Lett.*, **89**, 201502(2006).
- [22] Wen-feng Zhao, Jun-fang Chen, Ran Meng et al., *Applied Surface Science*, **256**, 2009 (2010).
- [23] Bogearts, A, Gijbels, R. *J. Appl. Phys.* **84**, 121(1998).
- [24] M. A. Lieberman, Lichtenber G A J., *Principles of plasma discharges and materials processing*. Wiley-Interscience, Malden. (1994).
- [25] H. U. Eckert, *High Temp. Sci.* **6**, 99(1974).
- [26] H. J. Yoon, T. H. Chung, Chung C J, *Thin Solid Films* **506- 507**, 454(2006).

*Corresponding author: zwf555@scau.edu.cn